Anisotropic resonant diffraction from $HoFe_2$

2001 J. Phys.: Condens. Matter 13 1891

(http://iopscience.iop.org/0953-8984/13/9/312)

INSTITUTE OF PHYSICS PUBLISHING JOURNAL OF PHYSICS: CONDENSED MATTER

J. Phys.: Condens. Matter **13** (2001) 1891–1905 www.iop.org/Journals/cm PII: S0953-8984(01)15708-5

Anisotropic resonant diffraction from $HoFe_2$

S P Collins[1], D Laundy[1] and A Stunault[2,3]

[1] Synchrotron Radiation Division, Daresbury Laboratory, Warrington WA4 4AD, UK
[2] XMaS, the UK CRG at the ESRF, BP 220, F-38043 Grenoble Cédex, France, and Department of Physics, University of Liverpool, Liverpool L69 7ZE, UK

E-mail: s.p.collins@daresbury.ac.uk

Received 21 July 2000, in final form 22 November 2000

Abstract

We have measured the energy and polarization dependence of anisotropic resonant x-ray Bragg diffraction from cubic $HoFe_2$ at glide-reflection-forbidden settings. Azimuthal scans at the iron K-edge are found to be consistent with calculations based on purely dipolar transitions. The possible influence of magnetic scattering is discussed, and we set out a simple procedure for calculating resonant intensities, based on crystal symmetry.

1. Background

Space-group extinction-rules in x-ray diffraction, for screw rotations and glide reflections, occur when beams scattered from equivalent atoms with different positions and *orientations*, cancel exactly. This relies on scattering being isotropic, which is the case for both non-resonant scattering, and resonant scattering from atoms in highly symmetric environments. There are, however, a great many examples of non-isotropic atomic resonances, leading to dichroic absorption [1] and anisotropic resonant scattering [2–11]. In such cases, the extinction rules must be treated as approximations. While absorption is governed by the overall symmetry of a crystal, resonant diffraction is sensitive to the *local* symmetry of individual atoms. This allows, for example, dipolar anisotropy to influence diffraction even in cubic crystals, as long as the site symmetry of the resonant atoms is non-cubic.

The present work concerns space-group-forbidden reflections in a cubic crystal and, specifically, dipole resonances from atoms at non-cubic sites. We have carried out diffraction measurements at the iron K-shell absorption-edge resonance in cubic $HoFe_2$ (space group $Fd\bar{3}m$), in which the iron atoms occupy sites of trigonal (rhombohedral) symmetry ($\bar{3}m$), and those of holmium take up cubic ($\bar{4}3m$) positions [12]: see figure 1.

The resonant contribution to the scattering amplitude arises from the $\boldsymbol{p} \cdot \boldsymbol{A}$ interaction, taken to second-order in perturbation theory ($\boldsymbol{p}$ and $\boldsymbol{A}$ represent the electron momentum

[3] Present address: Institut Laue–Langevin, BP 156, 38042 Grenoble Cedex 9, France.

0953-8984/01/091891+15$30.00

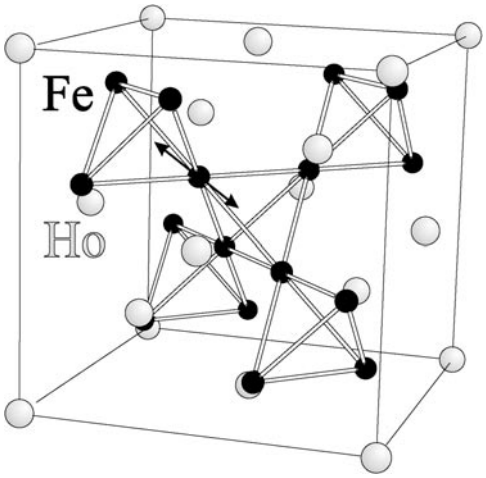

Figure 1. The $HoFe_2$ cubic unit cell. Iron tetrahedra are shown, and the threefold axis of one iron atom is indicated by an arrowed line.

and photon vector potential operators). This leads to an electric resonant amplitude [9, 13] expressible in terms of the position operator, $\boldsymbol{r}$,

$$f(\hbar\omega) \propto \sum_v \frac{\langle a|\boldsymbol{r}\cdot\boldsymbol{\varepsilon}'^{*}\,\mathrm{e}^{-\mathrm{i}\boldsymbol{q}'\cdot\boldsymbol{r}}|b_v\rangle\langle b_v|\boldsymbol{r}\cdot\boldsymbol{\varepsilon}\,\mathrm{e}^{\mathrm{i}\boldsymbol{q}\cdot\boldsymbol{r}}|a\rangle}{E_a - E_{b_v} + \hbar\omega - \mathrm{i}\Gamma/2} \tag{1}$$

where $\boldsymbol{\varepsilon}$, $\boldsymbol{\varepsilon}'$ are the polarization unit vectors of the incident and scattered beams, Γ is the core-hole lifetime and the sum runs over all intermediate states, $|b_v\rangle$. Writing the exponentials as Taylor series provides a multipole expansion of the scattering amplitude, of which the first (pure dipolar) term is

$$f(\hbar\omega) \propto \varepsilon_i\varepsilon_j'^{*}\left(\sum_v \frac{\langle a|r_j|b_v\rangle\langle b_v|r_i|a\rangle}{E_a - E_{b_v} + \hbar\omega - \mathrm{i}\Gamma/2}\right) = \varepsilon_i\varepsilon_j'^{*}T_{ij}. \tag{2}$$

Here, T_{ij} is a rank-two, energy-dependent tensor, ε_i and ε'_j are Cartesian components of the polarization unit vectors and we follow the Einstein convention for implied summations in a tensor expression. Complex conjugation of the secondary beam polarization vector will be omitted subsequently, since we employ purely real polarization vectors. Neglecting magnetism, the scattering tensor is symmetric with respect to exchange of indices i, j. Higher-order terms in the multipole expansion of (1) are described by tensors of higher rank, involving the vectors $\boldsymbol{q}$ and $\boldsymbol{q}'$ [9, 13].

The symmetric rank-two tensor outlined above contains, in general, six independent elements, equivalent to resonance responses along three perpendicular principal axes, and three orienting angles. For atoms in highly symmetric environments this number reduces dramatically, and the orientation and polarization dependence of the diffracted beams is governed largely or entirely by the symmetry of the resonant ions. The spectrum of resonant scattering requires a detailed knowledge of the electronic wavefunctions, and is beyond the scope of this paper.

2. Measurements and experimental results

All experimental results were obtained at the European Synchrotron Radiation Facility using the UK CRG beamline [14], with preliminary data obtained on SRS Station 16.3,

Daresbury Laboratory [15]. The sample, a 2 mm single-crystal cube grown by the Czochralski method at the University of Birmingham [16], was from the same batch of material as adopted for several previous measurements [12, 17]. The experimental layout and key parameters are indicated in figure 2 and table 1.

Table 1. Some key experimental parameters for the present work.

Sample dimensions	$2 \times 2 \times 2$ mm^3
Sample surface orientation	001
Sample reflection (mosaic) width	$\sim 0.02^\circ$
Photon linear polarization (P_3)	0.99
Monochromator	Si 111
Monochromator energy resolution	$\sim$ 1 eV
Fe K-edge energy	7.112 keV
Ho L_3-edge energy	8.071 keV
Polarization analyser reflection	Cu 220
Polarization analyser d-spacing	1.278 Å
Polarization analyser Bragg angle @ 7.112 keV	43.0°

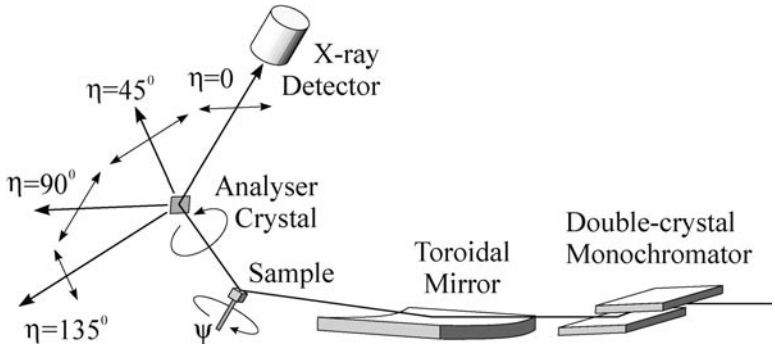

Figure 2. A schematic diagram of the experimental layout.

The present measurements, performed at ambient temperature and pressure, were concerned mainly with the 002 and 204 forbidden reflections. These are characterized by a strong dependence on both azimuthal angle (ψ) and photon energy. For each reflection, a series of ψ-scans (rotations about the scattering vector) was performed at the peak in the energy spectrum, and the energy scans taken over a range of ψ values close to maximum intensity. The highest 002 intensity ($\psi = 45^\circ$, energy $\sim$7.112 keV) was found to be $\sim$0.3% of that of the allowed 004 at the same energy.

Both the energy and ψ-scan data were affected by strong multiple scattering, so considerable effort was spent in order to minimize these features without prejudicing the extracted intensities. The 002 ψ-scan integrated intensities, obtained by fitting pseudo-Voigt functions to measured rocking curves, are shown in figure 3 after rejecting data points which deviate significantly from the medians of peak centroid and/or width. No data were rejected on the grounds of intensity. The results show clear fourfold symmetry, centred around $\psi = 0$, with the intensity minima being small, but not zero.

Removal of multiple scattering from the resonant energy spectra was harder to achieve since only peak intensities were recorded at each point. We were, however, able to make use of the fact that all of the 002 and 204 spectra appeared to exhibit the same shape, apart from

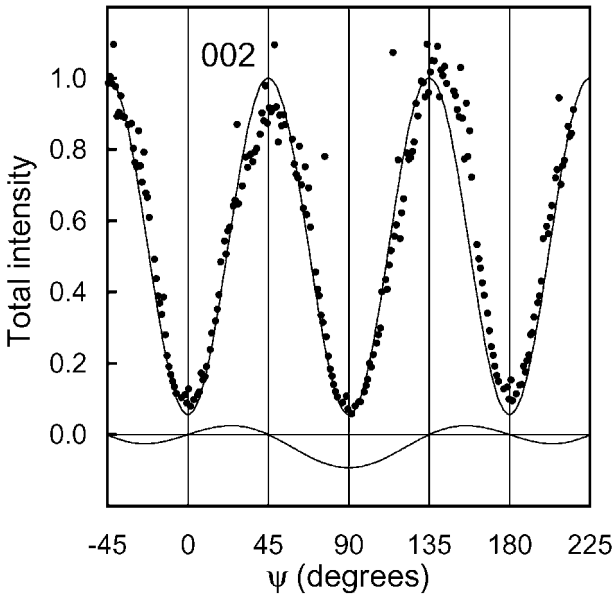

Figure 3. An azimuthal scan about the 002 reflection, at the peak of the iron K-edge resonance. The total diffraction intensities are scaled to best match the calculated intensity curve (solid line). $\psi = 0$ with the 100 vector normal to the scattering plane. Also shown is the calculated curve for magnetic/non-magnetic interference scattering for [010] domains (arbitrary scale), based on the magnetic structure described in section 4.

apparently random, rapid excursions, arising from multiple diffraction. After normalizing each spectrum to the height of the second strongest resonance peak at 7.123 keV, we combined the spectra using the following algorithm. First, calculate the mean spectrum by averaging all of the individual spectra. Then, from the set of intensities at each energy used to compute the mean, remove the data point furthest from the mean if it differs by more than 25% of that value. Finally, repeat this process until there are no further changes. This approach has the advantage that no assumptions are made about the mean intensity values, either on an absolute scale or in relation to neighbouring points in the spectrum. The only assumptions required are that (1) the single-scattering intensities for each energy have a symmetric probability distribution (e.g. a normal distribution), and (2) the multiple-scattering intensities have a wider distribution, which is flat over the $\pm 25\%$ acceptance window. By this method, we were able to extract the resonance spectrum well into the 'extended x-ray absorption' region (figure 4). Interestingly, the near-edge region seemed to show greater consistency than the higher energy part, although this may be due to the presence of more multiple scattering in the (wider) upper part of the spectrum, combined with the relatively weak resonant signal.

An absorption correction was applied to the resonance spectrum by multiplying the data by the total attenuation coefficient, obtained from transmission through powdered $HoFe_2$, brushed onto adhesive tape. The variation in absorption correction was modest due to strong attenuation by the holmium, and amounted to no more than 35%.

In addition to the total diffraction intensity, we measured the intensity through a Cu 220 polarization analyser, set to select linear polarization at angles of $\eta = 0$, 45, 90 and 135° with respect to $(\boldsymbol{q}' \times \boldsymbol{q})$. (Note that $\eta = 0°$ corresponds, in the limit of complete incident-beam polarization, to the σ–σ channel, and $\eta = 90°$ to σ–π). Azimuthal (ψ) scans, performed at the 002 and 204 reflections with each of the four polarizer settings, are shown in figures 5

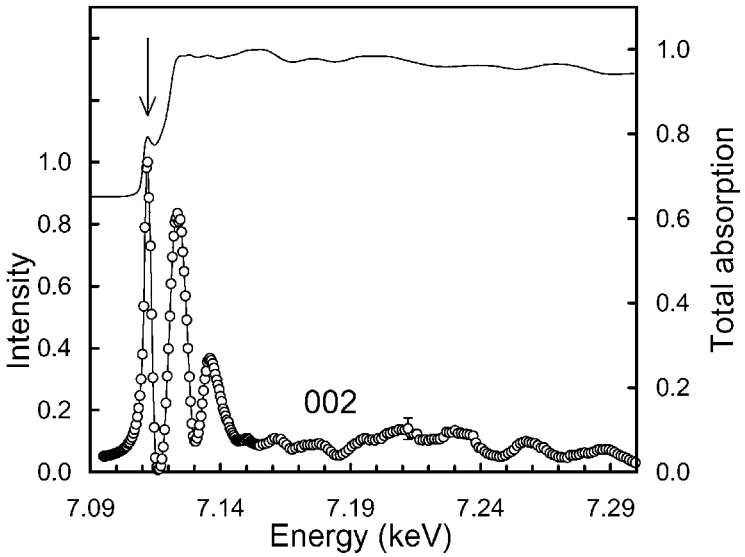

Figure 4. The energy spectrum of the total 002 diffraction intensity near the iron K-edge, corrected for sample absorption variations. The error bar is an estimate of the uncertainty in the extended ($>\sim$7.14 keV) part of the spectrum. Considerably greater reproducibility was found in the near-edge region. The energy at which the reported azimuthal scans were performed is indicated with an arrow. Also shown is the (normalized) absorption spectrum.

and 6. The data are given to within a single scaling factor for each reflection. No absorption corrections have been applied although, in principle, the 204 data are modified slightly by absorption changes. No intensity was detected above the multiple-diffraction 'background' at the holmium L_3 resonance energy for either the 002 or 204 settings.

3. Diffraction intensities: comparison with calculations

The azimuthal dependence of total diffraction intensities (figure 3) and polarized intensities (figures 5 and 6) are all found to be in good agreement with calculations based on the following assumptions: (1) the dipole approximation is valid, (2) magnetic scattering is relatively weak and (3) perturbation of the $Fd\bar{3}m$ crystal symmetry, due to magnetoelastic strain, is negligible. Of these three assumptions, the first—the dipole (E1) approximation—is perhaps the most contentious, as quadrupole (E2) excitations, leading to scattering tensors of rank three and four, have been observed in similar experiments [4, 5, 8]. No such effects were seen here, either in the azimuthal or energy scans.

The structure-factor tensors for electric dipole resonances at forbidden reflections, derived in the appendix, are symmetric, traceless rank-two tensors. For the iron site in $HoFe_2$, the tensor elements scale with a single resonant strength, b, for example

$$F_{002} = 16\mathrm{i}b \begin{pmatrix} 0 & 1 & 0 \\ 1 & 0 & 0 \\ 0 & 0 & 0 \end{pmatrix}.$$

All intensities scale with $|b|^2$. Calculated ψ-scan intensities can therefore be compared with the experimental data simply by multiplying the data from each set of measurements by a single scale factor. These factors were derived graphically, and are essentially values which cause the largest number of data points to lie close to the calculated curves. Such a procedure

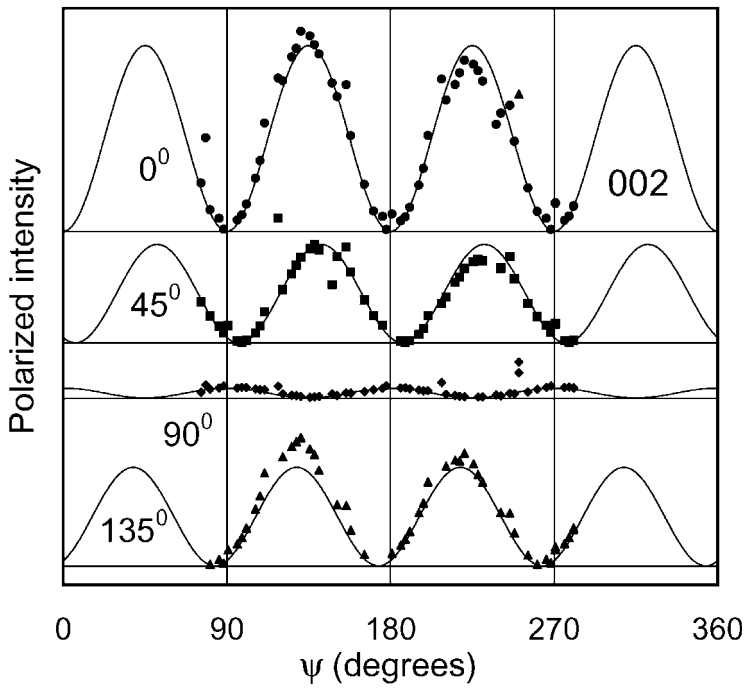

Figure 5. Azimuthal scans about the 002 reflection, measured with the linear polarization analyser set to angles of 0, 45, 90 and 135° from horizontal (σ). The data are all scaled by a single factor for comparison with calculated curves (solid lines). Intensities are plotted on a linear scale, with horizontal lines representing zero for each data set.

was considered preferable to a more conventional least-squares approach because a significant number of intensity readings are dominated by strong multiple scattering effects, and lie very far from neighbouring points (with several outside the displayed axis limits of the graphs). The small departures from calculated curves are likely to arise from systematic experimental errors, including effects of saw-marks on the sample surface and imperfections in the polarization analyser. The discrepancies do not follow the calculated forms for either magnetic scattering (see section 4) or higher-order multipole resonances (discussed in the appendix).

It is instructive to consider the properties of the symmetric tensor that describes anisotropic resonant scattering within the dipole approximation. The structure factor tensor can be written as the sum of an isotropic (scalar) part F_I, and a symmetric anisotropic part with zero trace, F_S:

$$F = F_I + F_S. \tag{3}$$

F_I gives diffraction which is independent of the azimuthal angle, ψ, whereas F_S produces a strong ψ-dependence, but tends to be much smaller in magnitude. One finds that the structure factor tensor belongs to one of four possible classes:

(1) $F = 0$ strictly forbidden reflection
(2) $F = F_I$ isotropic tensor—allowed reflection
(3) $F = F_S$ anisotropic tensor—weak reflection
(4) $F = F_I + F_S$ mixed tensor—allowed, weakly anisotropic.

Most of the diffraction measurements in this work belong to class (3), but all four classes are represented by Bragg reflections in $HoFe_2$, as seen in table 2. Note that the holmium

Table 2. Properties of the symmetric rank-two structure factor tensors for the iron and holmium sites in $HoFe_2$. The tables indicate non-vanishing isotropic (F_I) and symmetric anisotropic (F_S) components.

	Iron	Holmium
$0, 0, l$ & $l, 0, 2l$ reflections		
$l =$ odd	0	0
$l = 2n, n =$ odd	F_S	0
$l = 2n, n =$ even	F_I	F_I
h, h, h reflections		
$h =$ odd	$F_I + F_S$	F_I
$h = 2n, n =$ odd	F_I	0
$h = 2n, n =$ even	F_I	F_I

structure factor tensors are purely isotropic. This is because only isotropic rank-two tensors can exist in the cubic site symmetry ($\bar{4}3m$) of the holmium atoms. The ratio of the maximum 002 intensity ($\psi = 45^\circ$) to that of the 004 (a class 2 reflection of modest intensity) is found to be

$$\frac{I_{002}}{I_{004}} = \frac{\sin(2\theta_{004})}{\sin(2\theta_{002})} \frac{4|b|^2}{|f_{Ho} - 2f_{Fe}|^2}. \tag{4}$$

Equating this to the measured 0.3% intensity ratio, and using tabulated atomic form factors [18], we obtain the result, $|b|_{max} \sim 0.5$ electrons. This value is approximately twice that reported for FeS_2 [8], although the present result is very sensitive to uncertainties in f'_{Fe} close to resonance. We estimate f'_{Fe} from [19] to be around -6 electrons.

4. Magnetic scattering

Although the experimental data from $HoFe_2$ seem to be well described by a simple model which requires only a symmetric dipole resonance at the Fe K edge, it must be remembered that the material is ferromagnetic—a fact which is inconsistent with a strict adherence to the $Fd\bar{3}m$ space-group symmetry. Here, we consider briefly the possible effects of magnetic scattering on the measured intensities.

Assuming that the magnetic vectors in $HoFe_2$ lie along one of the six $\langle 100 \rangle$ directions, the simplest modification to the present model is a collinear magnetic structure with each Fe spin (we consider only the iron resonance) aligned with the bulk magnetization [20]. However, such a magnetic component would be subject to the usual extinction rules and would not produce a signal at the forbidden 002 or 204 reflections.

One could consider an alternative structure for at least a *component* of the magnetism which is consistent with the non-magnetic crystal symmetry. In order to admit the possibility of a net magnetic moment, those (half) of the space-group operators which turn the spin away from the magnetic vector are combined with the time-reversal operator, which reverses the spin direction. For the rank-two case, which we consider here, the time-reversal operator transposes the two tensor indices. This clearly effects only the antisymmetric part of the tensor, which is identified with an axial vector along the local spin direction. Considering the iron atom at $(1/8, 3/8, 7/8)$, the magnetic part of the atomic scattering is found to be of the form

$$T = \pm A \begin{pmatrix} 0 & -1 & 1 \\ 1 & 0 & 1 \\ -1 & -1 & 0 \end{pmatrix} \tag{5}$$

which corresponds to a $\pm(1, -1, -1)$ spin vector, aligned with the threefold axis. The antisymmetric structure factor tensors for the forbidden 200 reflection, resulting from

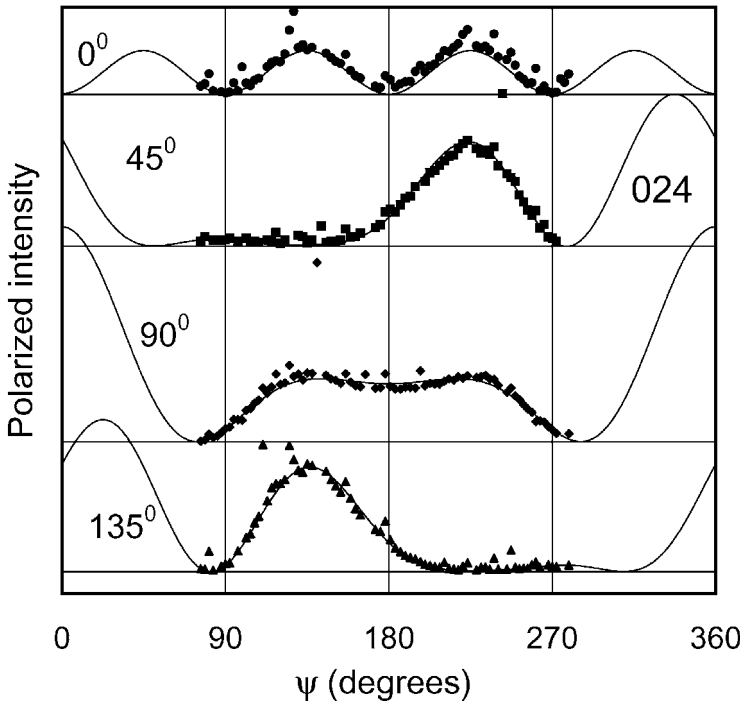

Figure 6. As figure 5, for the 204 reflection.

space-group operators modified to produce a net moment along each of the six magnetic vectors $\boldsymbol{m}$, are then

$$F_{002} = \pm 16\mathrm{i}A \begin{pmatrix} 0 & 0 & -1 \\ 0 & 0 & 0 \\ 1 & 0 & 0 \end{pmatrix}, \qquad \pm 16\mathrm{i}A \begin{pmatrix} 0 & 0 & 0 \\ 0 & 0 & -1 \\ 0 & 1 & 0 \end{pmatrix}, \qquad 0 \qquad (6)$$

for $\boldsymbol{m} = (\pm 1, 0, 0)$, $(0, \pm 1, 0)$ and $(0, 0, \pm 1)$, respectively. (Note that the magnetic scattering vanishes when the magnetic axis is aligned with the scattering vector.) The diffraction intensities for mixed magnetic/non-magnetic (asymmetric) tensors contain non-magnetic terms, purely magnetic terms and terms arising from interference between the magnetic and non-magnetic amplitudes. Although each of these exhibits a characteristic azimuth dependence, an equal population of the six magnetic domains produces a magnetic intensity which is independent of sample rotation.

Since the measured intensity curves (figures 3, 5 and 6) show a slight deviation from the predictions of the non-magnetic model, one might suspect a contribution from magnetic scattering, arising from an uneven domain distribution. However, neither the purely magnetic, nor the interference terms, fit the bill in terms of shape (the latter are shown with the data in figure 3). Finally, it is interesting to note that the above model for magnetism in $HoFe_2$ would result in some pure magnetic reflections (including the 002) in a neutron diffraction experiment.

5. Summary and conclusions

The total and linearly polarized intensities of anisotropic resonant scattering from glide-reflection-forbidden diffraction in $HoFe_2$ have been measured in the vicinity of the iron

K-shell absorption edge. By far the most severe experimental complication afflicting such measurements arises from multiple diffraction, which produces intensities at forbidden reflection settings. We have shown that such effects, which tend to be either negligible or to exhibit very strong and apparently random intensity fluctuations with energy and azimuth, can be minimized in a systematic way. We have thus obtained an extended energy spectrum of the iron K-edge resonance, as well as high-quality data on the azimuth (ψ)-dependence of both the total and linearly polarized diffraction intensities from the 002 and 204 reflections.

All ψ-scans have been found to be in excellent accord with calculations based on pure electric dipole resonances. We observed no evidence for quadrupolar features in either the energy spectra or azimuth dependence. Neither was any signal detected, above the multiple scattering 'background', at the 002 or 204 reflections near the holmium L_3-edge resonance.

The absence of non-dipolar effects seems a little surprising, given that we find no obvious symmetry argument to rule them out, and that they are clearly evident in, for example, α-Fe_2O_3 [4] and FeS_2 [8]. (The latter exhibits an almost identical Fe K-edge dipole spectrum to the present case.) One possible explanation is simply that the light elements (e.g. sulphur and oxygen) cause little x-ray attenuation, and one observes strong intensity enhancement in the crucial pre-edge region of the energy spectrum [21]. In $HoFe_2$, on the other hand, strong absorption by holmium limits this enhancement to about 35%.

While modelling anisotropic resonant scattering is not especially difficult, it can become convoluted, particularly when exploring the effects of non-dipolar resonances. The appendices of this paper are devoted to a fairly detailed prescription for performing such calculations on non-magnetic crystals, requiring just the space-group generators from the *International Tables for Crystallography* [22] and atomic coordinates. We show how the total and polarized diffraction intensities can be computed for an arbitrary partial incident beam polarization (described by Stokes parameters) for dipole, quadrupole and mixed resonances.

Acknowledgments

The authors gratefully acknowledge the valuable help and assistance provided by the staff of the XMaS UK CRG beamline during the reported measurements, J S Abell, Y J Bi and D Fort, School of Metallurgy and Materials, University of Birmingham for producing the $HoFe_2$ crystals, and S W Lovesey and S J Teat for valuable discussions.

Appendix. Calculation of intensities and polarization of diffraction from a resonant ion in a non-magnetic crystal

This appendix sets out a simple, but quite general, approach to calculating the properties of diffraction from a resonant ion in a crystal of known (non-magnetic) space-group symmetry. Nine steps complete the calculation, starting from the properties of the relevant multipole scattering tensor, and ending with a two-dimensional scattering matrix, which is the basis for applying standard density matrix techniques (using Stokes parameters) to calculate the intensity and polarization of the scattered beam.

A.1. Generate a scattering tensor of the required rank and symmetry

Resonant multipole scattering amplitudes can be usefully expressed [5, 13] in terms of a Cartesian tensor, $T_{ijk}\ldots$, coupled to a set of vectors, which generally include $\boldsymbol{\varepsilon}$, $\boldsymbol{\varepsilon}'$, $\boldsymbol{k}$ and $\boldsymbol{k}'$. The rank of the tensor increases with multipolarity: rank 2 for pure dipole (E1E1), rank 3

for mixed dipole–quadrupole (E1E2), rank 4 for pure quadrupole etc. Table A1 lists the tensor formulae for the above processes.

Table A1. The form of the scattering amplitude, the tensor symmetries and the relationship between the scattering tensor and scattering matrix, for dipolar, quadrupolar and mixed dipole–quadrupole resonances [13]. All expressions apply to the tensors T and F; underlining indicates that time-reversal symmetry applies. The $*$ symbol marks tensor index permutations which correspond to time reversal.

	E1E1	E1E2	E2E2
Scattering amplitude	$\varepsilon_i \varepsilon'_j T_{ij}$	$\underline{(\varepsilon_i \varepsilon'_j q_k - \varepsilon'_i \varepsilon_j q'_k) T_{ijk}}$	$\varepsilon_i q_j \varepsilon'_k q'_l T_{ijkl}$
Tensor symmetries	$\underline{[2,1]^*}$	$\underline{[3,2,1]}$	$[2,1,3,4], [1,2,4,3], \underline{[3,4,1,2]^*}$
Scattering matrix	$M_{ij} = T_{ij}$	$\underline{M_{ij} = q_k T_{ijk} - q'_k T_{jik}}$	$M_{ij} = q_k q'_l T_{ikjl}$

The number of independent elements in these three-dimensional, rank N tensors can be less than 3^N due to inherent symmetries in the scattering processes, plus additional constraints arising from the assumption of time-reversal invariance [13] applicable to non-magnetic states. The net result is a tensor containing elements which are symmetric with respect to exchange of certain indices. These are listed in table A1.

As an example, the scattering tensor for a pure dipole (E1) resonance in a non-magnetic environment, is simply the symmetric rank-2 tensor,

$$T = \begin{pmatrix} a & b & c \\ b & d & e \\ c & e & f \end{pmatrix} \tag{A1}$$

where the six tensor elements are complex, energy-dependent quantities.

A.2. Generate the space group operators

The group, $\mathfrak{G}$, of spatial symmetry operators that act on a unit cell provide both the symmetry of the resonant ions, and the placement of all equivalent ions in the cell. These can be computed conveniently and quickly from the *space-group generators* listed in the *International Tables of Crystallography* [22],

$$\mathfrak{G} = \mathfrak{g}^n * \mathfrak{g}^{n-1} * \cdots * \mathfrak{g}^2 * \mathfrak{g}^1 \tag{A2}$$

with each subgroup $\mathfrak{g}^n$ formed by repeated application of the generator g^n. (We neglect the first four generators listed in the *International Tables*, which correspond to the identity and three unit cell translation vectors).

For the space-group $Fd\bar{3}m$ one obtains seven generators, of which the first (a centring translation) and last (an inversion) are written:

$$\begin{aligned} g^1 &= t(0, 1/2, 1/2) = \left(\begin{pmatrix} 1 & 0 & 0 \\ 0 & 1 & 0 \\ 0 & 0 & 1 \end{pmatrix}, \begin{pmatrix} 0 \\ 1/2 \\ 1/2 \end{pmatrix} \right) \\ g^7 &= (25) = \left(\begin{pmatrix} -1 & 0 & 0 \\ 0 & -1 & 0 \\ 0 & 0 & -1 \end{pmatrix}, \begin{pmatrix} 0 \\ 0 \\ 0 \end{pmatrix} \right). \end{aligned} \tag{A3}$$

The group generated by (A2) contains, as expected, $2 \times 2 \times 2 \times 2 \times 3 \times 2 \times 2 = 192$ element, which are identified with the 192 equivalent positions for the space group.

A.3. Generate the point group

The point group, $\mathfrak{P}$, for a particular site is readily obtained as the set of the rotational (proper and improper) parts of those elements of $\mathfrak{G}$ which preserve the position vector. Turning again to the present example of $HoFe_2$ there is, using origin choice 1 [22], an iron atom at $(1/8, 3/8, 7/8)$. The resulting 12-element point group, denoted by $\bar{3}m$, includes an inversion, a threefold axis and a mirror plane.

A.4. Generate the atomic scattering tensor

The next task is to ensure that the general scattering tensor in step 1 is invariant with respect to the point group $\mathfrak{P}$ by solving the set of equations,

$$P^n * T - T = 0. \tag{A4}$$

The unitary operators P^n which form the group $\mathfrak{P}$ transform the tensor T such that

$$P^n * T = P^n_{Ii} P^n_{Jj} P^n_{Kk} \cdots T_{ijk\ldots}. \tag{A5}$$

Application of (A4) to the iron atom in $HoFe_2$ results in the much simplified dipole scattering tensor,

$$T = \begin{pmatrix} a & b & b \\ b & a & b \\ b & b & a \end{pmatrix} \tag{A6}$$

which can be broken down into the sum of an isotropic part of amplitude a, and an anisotropic part of amplitude b. The latter represents the *difference* in response along, and perpendicular to, the threefold axis.

A.5. Generate the structure factor tensor

We next consider the tensor for (kinematical) diffraction from all the symmetry-related resonant atoms in a unit cell. For a given symmetry group $\mathfrak{G}$, relative atomic position $\boldsymbol{x}$ and reciprocal lattice vector $\boldsymbol{h}$, we sum over all the contributing tensors, taking into account differences in orientations and phases:

$$F_{\boldsymbol{k}} = \frac{1}{N} \sum_n (R^n * T)\, \mathrm{e}^{\mathrm{i}\phi} \tag{A7}$$

where $\phi = 2\pi \boldsymbol{h} \cdot (S^n * \boldsymbol{x})$. In the above expressions, the nth element S^n of the space group $\mathfrak{G}$ comprises a rotational part and a translational part, such that $S^n * \boldsymbol{x} = R^n \boldsymbol{x} + V^n$. The factor $1/N$ in (A7) accounts for symmetries at special positions in the unit cell, i.e., N is the number of symmetry operators that leave the atomic position invariant.

While it is both convenient and instructive to consider the point-group symmetry (step (4)) at the resonant ion, and its effect on the scattering tensor, all symmetries are, in fact, accounted for in the above expressions.

Applying (A7) to the present example of iron in $HoFe_2$ ($\boldsymbol{x} = (1/8, 3/8, 7/8)$, $\boldsymbol{h} = (0, 0, 2), (0, 0, 4), (2, 0, 4)$) one finds

$$F_{002} = 16\mathrm{i}b \begin{pmatrix} 0 & 1 & 0 \\ 1 & 0 & 0 \\ 0 & 0 & 0 \end{pmatrix} \qquad F_{004} = -16a \begin{pmatrix} 1 & 0 & 0 \\ 0 & 1 & 0 \\ 0 & 0 & 1 \end{pmatrix}$$

$$F_{204} = -16\mathrm{i}b \begin{pmatrix} 0 & 0 & 0 \\ 0 & 0 & 1 \\ 0 & 1 & 0 \end{pmatrix}. \tag{A8}$$

Table A2. The number of independent elements in the structure-factor tensor for three resonance processes (E1E1, E1E2, E2E2) at the reflections used for the present study.

	E1E1	E1E2	E2E2
Fe 002	1	0	3
Fe 204	1	0	3
Ho 002	0	1	0
Ho 204	0	1	0

It is clear from these results that the 004 reflection is isotropic, whereas the 002 and 204 reflections are totally anisotropic, and will depend on the directions of the incident and scattered beam polarizations with respect to the sample. (In fact, the 204 structure factor tensor, as given above, is not quite correct since it involves a rotation of the sample and, therefore, the structure factor tensor. The required transformation is discussed next.)

The structure-factor tensors for higher-order multipole resonances, and for the holmium site, have been calculated in a similar way. Although the results are not reproduced here, table A2 gives an overview by indicating the number of independent tensor elements in each case. The table gives no indication as to why no quadrupolar processes were observed during the present measurements.

A.6. Rotate the structure factor tensor

Adopting the coordinate system shown in figure A1, the atomic scattering tensor is expressed in terms of components along directions defined by $\boldsymbol{q}$, $\boldsymbol{q}'$. However, one often needs to employ a different frame of reference (for example, during a ψ-scan and/or when moving to a new reflection). In order to carry out the required coordinate transformations, it is convenient to define primary and secondary reflections, with momentum vectors $\boldsymbol{h}_0$ and $\boldsymbol{h}_1$, in terms of which the coordinate axes are

$$\hat{\mathbf{3}} = \hat{\boldsymbol{h}}_0 \qquad \hat{\mathbf{2}} = \frac{\hat{\boldsymbol{h}}_0 \times \hat{\boldsymbol{h}}_1}{|\hat{\boldsymbol{h}}_0 \times \hat{\boldsymbol{h}}_1|} \qquad \hat{\mathbf{1}} = \hat{\mathbf{2}} \times \hat{\mathbf{3}}. \tag{A9}$$

The scattering/structure factor tensor for an arbitrary secondary reflection, with an azimuthal angle ψ, is then

$$F \rightarrow R_3(\psi) R_2(\alpha) * F \tag{A10}$$

where

$$R_3(\psi) = \begin{pmatrix} \cos(\psi) & -\sin(\psi) & 0 \\ \sin(\psi) & \cos(\psi) & 0 \\ 0 & 0 & 1 \end{pmatrix} \qquad R_2(\alpha) = \begin{pmatrix} \cos(\alpha) & 0 & \sin(\alpha) \\ 0 & 1 & 0 \\ -\sin(\alpha) & 0 & \cos(\alpha) \end{pmatrix} \tag{A11}$$

and α is the angle between $\boldsymbol{h}_0$ and $\boldsymbol{h}_1$. For an azimuthal rotation about the primary reflection, one simply takes $\alpha = 0$. In the present work, the primary and secondary reflections are taken as 002 and 204. This means that $\hat{\mathbf{1}}$, $\hat{\mathbf{2}}$ and $\hat{\mathbf{3}}$ lie conveniently along the edges of the cubic unit cell.

A.7. Generate the three-dimensional scattering matrix

With the exception of the pure dipolar rank-two case, the scattering tensors couple to the vectors $\boldsymbol{q}$, $\boldsymbol{q}'$. Since all of the necessary tensor transformations have already been performed, it is convenient at this stage to couple the tensors to these well defined vectors. The scattering

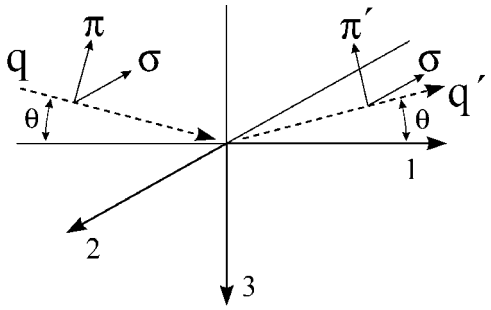

Figure A1. The coordinate system adopted for the present work (from [23]).

amplitude, M, is then described by a three-dimensional matrix, which depends only on the photon polarization vectors ε, ε'. The resulting matrices for E1E1, E1E2 and E2E2 processes are summarized in table A1.

A.8. Generate the two-dimensional scattering matrix

Calculations of intensities and scattered-beam polarization can be performed conveniently using the two-dimensional scattering amplitude matrix [24], expressed in terms of orthogonal linear polarization states of both the incident and scattered beams, perpendicular (σ) and parallel (π) to the scattering plane.

In order to obtain the two-dimensional scattering amplitude from M, we employ two projection matrices,

$$\Gamma = \begin{pmatrix} 0 & 1 & 0 \\ \sin(\theta) & 0 & \cos(\theta) \end{pmatrix} \qquad \Delta = \begin{pmatrix} 0 & -\sin(\theta) \\ 1 & 0 \\ 0 & \cos(\theta) \end{pmatrix} \tag{A12}$$

in terms of which the 2D scattering amplitude matrix is

$$G = \Gamma M \Delta. \tag{A13}$$

Referring again to the 002 and 004 reflections of $HoFe_2$, we find, for a dipolar resonance,

$$G_{002} = 16ib \begin{pmatrix} \sin(2\psi) & -\sin(\theta)\cos(2\psi) \\ \sin(\theta)\cos(2\psi) & \sin^2(\theta)\sin(2\psi) \end{pmatrix} \qquad G_{004} = -16a \begin{pmatrix} 1 & 0 \\ 0 & \cos(2\theta) \end{pmatrix}.$$

The 004 matrix has the familiar form for isotropic scattering (arising from the product of the projection matrices in (A12)). On the other hand, the scattering matrix for 002 depends on the azimuthal orientation of the sample. For $\psi = 0$ only off-diagonal elements are present, indicating a complete rotation of the linear polarization states. At $\psi = \pm\pi/4$ the matrix is diagonal, with no polarization rotation. The scattering matrix for the 204 reflection more complex, depending on θ, ψ and α.

A.9. Intensity calculations

Armed with the appropriate scattering matrix, we can now employ standard techniques for calculating the diffracted intensity with an arbitrary (partial) beam polarization. To this end, we write the polarization density matrix for the incident beam [24] as

$$\mu = \frac{1}{2} \begin{pmatrix} 1 + P_3 & P_1 - \mathrm{i}P_2 \\ P_1 + \mathrm{i}P_2 & 1 - P_3 \end{pmatrix} \tag{A14}$$

where $P_{1,2,3}$ are, respectively, the degrees of linear polarization at 45° from a plane of scattering, the mean helicity (circular polarization), and linear polarization normal to the scattering plane. The kinematical diffraction intensity for any polarization state is then simply the trace of the product of three matrices,

$$I \propto \mathrm{Tr}(G\mu G^{\dagger}). \tag{A15}$$

where similarly, the Stokes parameter P_i for the scattered beam is

$$P_i = \frac{\mathrm{Tr}(\sigma_i G\mu G^{\dagger})}{\mathrm{Tr}(G\mu G^{\dagger})} \tag{A16}$$

where † indicates a Hermitian conjugate and the Pauli matrices, σ_i, are defined in [24].

We are now able to completely characterize the intensity and polarization of the diffracted beam, with any sample orientation. While the expressions evaluated via (A15) and (A16) are, in general, too lengthy to be usefully expanded on paper, some simplified cases are more manageable. Taking $P_1 = P_2 = 0$, $P_3 = +1$, we find

$$I_{002} = (16b)^2(1 - \cos^2(\theta)\cos^2(2\psi))$$

which, for small values of θ, reduces to $I_{002} \propto \sin^2(2\psi)$. (This can be compared with the results in figure 3.)

The final calculation of interest is of the diffracted intensity which passes though a (less than perfect) linear polarization analyser. The response of such a device, based on kinematic diffraction through angles close to 90°, is outlined in [25], and takes the form of a second scattering amplitude matrix,

$$A = \begin{pmatrix} \cos(\eta) & -\sin(\eta) \\ \cos(2\phi)\sin(\eta) & \cos(2\phi)\cos(\eta) \end{pmatrix} \tag{A17}$$

where ϕ is the Bragg angle for the analyser crystal, and η is the angle between the scattering planes of the sample and analyser. The new scattering matrix simply operates on G to provide the net scattering amplitude matrix for sample and analyser, i.e. $G \rightarrow AG$, leading to an intensity of the form

$$I \propto \mathrm{Tr}(AG\mu G^{\dagger}A^{\dagger}). \tag{A18}$$

References

[1] Brouder C 1990 *J. Phys.: Condens. Matter* **2** 701–38
[2] Dmitrienko V E 1984 *Acta Crystallogr.* A **40** 89–95
[3] Kirfel A, Petcov A and Eichhorn K 1991 *Acta Crystallogr.* A **47** 180–95
[4] Finkelstein K D, Shen Q and Shastri S 1992 *Phys. Rev. Lett.* **69** 1612–15
[5] Templeton D H and Templeton L K 1994 *Phys. Rev.* B **49** 14 850–53
[6] Nagano T, Kokubun J, Yazawa I, Kurasawa T, Kuribayashi M, Tsuji E, Ishida K, Sasaki S, Mori T, Kishimoto S and Murakami Y 1996 *J. Phys. Soc. Japan* **65** 3060–7
[7] Templeton D H and Templeton L K 1997 *Acta Crystallogr.* A **53** 352–5
[8] Kokubun J, Nagano T, Kuribayashi M and Ishida K 1998 *J. Phys. Soc. Japan* **67** 3114–18
[9] Templeton D H 1998 *Acta Crystallogr.* A **54** 158–62
[10] Hagiwara K, Kanazawa M, Horie K, Kokubun J and Ishida K 1999 *J. Phys. Soc. Japan* **68** 1592–7
[11] Carra P and Thole B T 1994 *Rev. Mod. Phys.* **66** 1509–15
[12] Streltsov V A and Ishizawa N 1999 *Acta Crystallogr.* B **55** 321–6
[13] Blume M 1994 *Resonant Anomalous X-Ray Scattering* ed G Materlik, C J Sparks and K Fischer (Amsterdam: North-Holland)
[14] Brown S D, Cooper M J, Kervin J, Paul D F, Stirling W G, Stunault A and Thompson P 2001 *Nucl. Instrum. Methods* to be published
[15] Collins S P, Cernik R J, Fell B, Tang C C, Harris N W, Miller M C and Oszlanyi G 1998 *J. Synchrotron Radiat.* **5** 1263–9

[16] Bi Y J, Abell J S and Hwang A M H 1991 *J. Magn. Magn. Mater.* **99** 159–66
[17] Collins S P, Laundy D and Guo G Y 1993 *J. Phys.: Condens. Matter* **5** L637
[18] Wilson A J C and Prince E (eds) 1989 *International Tables for X-Ray Crystallography* vol C (Dordrecht: Kluwer)
[19] Begum R, Hart M, Lea K R and Siddons D P 1986 *Acta Crystallogr.* A **42** 456–64
[20] Fuess H, Givord D, Gregory A R and Schweizer J 1979 *J. Appl. Phys.* **50** 2000–2
[21] Dräger G, Frahm R, Materlik G and Brümmer O 1988 *Phys. Status Solidi* b **146** 287–94
[22] Hahn T (ed) 1987 *International Tables for Crystallography* vol A (Dordrecht: Kluwer)
[23] Hill J P and McMorrow D F 1996 *Acta Crystallogr.* A **52** 236–44
[24] Lovesey S W 1987 *J. Phys. C: Solid State Phys.* **20** 5625–39
[25] Collins S P 1999 *J. Phys.: Condens. Matter* **11** 1159–75